Modeling relativistic soliton interactions in overdense plasmas: A perturbed nonlinear Schrödinger equation framework

E. Siminos,[1,*] G. Sánchez-Arriaga,[2] V. Saxena,[3] and I. Kourakis[4]

[1]*Max Planck Institute for the Physics of Complex Systems, Nöthnitzer Strasse 38, D-01187 Dresden, Germany*

[2]*Departamento de Física Aplicada, Escuela Técnica Superior de Ingenieros Aeronáuticos, Universidad Politécnica de Madrid, Madrid, Spain*

[3]*Centre for Free-Electron Laser Science, Deutsches Elektronen-Synchrotron, Notkestrasse 85, 22607 Hamburg, Germany*

[4]*Centre for Plasma Physics, School of Mathematics and Physics, Queen's University Belfast, Belfast BT7 1NN, Northern Ireland, United Kingdom*

(Received 2 October 2014; published 3 December 2014)

We investigate the dynamics of localized solutions of the relativistic cold-fluid plasma model in the small but finite amplitude limit, for slightly overcritical plasma density. Adopting a multiple scale analysis, we derive a perturbed nonlinear Schrödinger equation that describes the evolution of the envelope of circularly polarized electromagnetic field. Retaining terms up to fifth order in the small perturbation parameter, we derive a self-consistent framework for the description of the plasma response in the presence of localized electromagnetic field. The formalism is applied to standing electromagnetic soliton interactions and the results are validated by simulations of the full cold-fluid model. To lowest order, a cubic nonlinear Schrödinger equation with a focusing nonlinearity is recovered. Classical quasiparticle theory is used to obtain analytical estimates for the collision time and minimum distance of approach between solitons. For larger soliton amplitudes the inclusion of the fifth-order terms is essential for a qualitatively correct description of soliton interactions. The defocusing quintic nonlinearity leads to inelastic soliton collisions, while bound states of solitons do not persist under perturbations in the initial phase or amplitude.

DOI: 10.1103/PhysRevE.90.063104 PACS number(s): 52.27.Ny, 52.35.Sb, 52.38.−r, 52.65.−y

I. INTRODUCTION

The availability of short, intense laser pulses has opened new regimes of laser-plasma interaction, rendering possible the excitation and study of various localized structures in the plasma. Amidst a plethora of excitations observed, a particular role is played by electromagnetic solitons, i.e., self-trapped pulses characterized (and sustained) by a balance of dispersion or diffraction and nonlinearity. In particular, we shall be interested in so-called relativistic solitons, for which the electromagnetic field amplitude is intense enough to set plasma electrons in relativistic motion.

Relativistic solitons have been predicted by analytical theory [1–5] and simulations [6–11], and their signatures have been observed in experiments [12–18]. They can be thought of as electromagnetic pulses trapped in a plasma density cavitation with overdense boundaries. For one-dimensional (1D) plasma geometry, a vast number of soliton families have been identified and studied [5,19,20,20–22], while higher-dimensional solitons have also been encountered in simulations [9,23]. In overdense plasmas near the critical density, solitons can be excited by a long intense pulse incident on a plasma density gradient [2,11]. In underdense plasmas, relativistic solitons have been observed behind the wake left by an intense and short pulse [8–10,23]. In this case, soliton creation is linked to the downshift of the laser pulse frequency as it propagates through the plasma, which leads to an effective reduction of the critical density and trapping of laser pulse energy in the form of a soliton [23]. Therefore, from this point on, we will use the term overdense plasma in association to the frequency ω of the soliton. The latter may be lower than the frequency of the laser pulse that excited the soliton.

Simulations [7,11,23] and experiments [12,13] show that multiple solitons may be excited by a single laser pulse, and one may expect that these solitons can interact with each other [23]. In a previous publication [24] we presented numerical studies of interactions of standing electromagnetic solitons of the form predicted in Ref. [5], within the relativistic cold-fluid framework. For low soliton amplitudes, a phenomenology similar to nonlinear Schrödinger (NLS) equation soliton interaction [25] has been observed, e.g., involving the formation of bound states, under certain circumstances. However, soliton interaction for larger amplitudes departs from NLS equation phenomenology.

The aim of the present work is to gain more insight in the origin of the NLS equation behavior of small amplitude soliton interaction in overdense plasmas but also to explore how deviations from NLS equation behavior arise. Starting from the one-dimensional relativistic cold-fluid model, we develop a perturbative treatment based on multiple scale analysis [26–28], in which the small parameter is the electromagnetic field amplitude. Under the assumptions of immobile ions and circular polarization we derive a perturbed NLS-type equation (pNLS equation), which describes the evolution of the electromagnetic field envelope. In our expansion, localization of the soliton solution is introduced naturally as a result of the assumption of a carrier frequency ω smaller but similar to the plasma frequency, $\omega \lesssim \omega_{\mathrm{pe}} = \sqrt{N_0 e^2/m_e\epsilon_0}$, where N_0 is the plasma background density, m_e is the electron rest mass, $-e$ is the electron charge, and ϵ_0 is the permittivity of free space. The dominant nonlinear term is a "focusing" cubic nonlinearity, while at higher order a "defocusing" quintic one also appears. They both result from the perturbative expansion

*evangelos.siminos@gmail.com

of the relativistic γ factor. Additional higher-order nonlinear terms result from the ponderomotive coupling of the field to the plasma. To lowest order our pNLS equation reduces to a focusing NLS equation.

Our study of soliton interactions using the fluid and pNLS equation models shows that soliton collisions are inelastic. This is commonly regarded as a signature of nonintegrability of the governing equations [29] and is in stark contrast with the elastic collisions of solitons of the (integrable) cubic NLS equation. We note that although a distinction between solitary waves and solitons based on the nature of their interactions can be made [30], here we adhere to the common practice in laser-plasma interaction literature of referring to any solitary wave solution as a soliton.

The NLS equation is ubiquitous in physics since it appears generically as an envelope equation describing propagation of weakly nonlinear waves in dispersive media [27,28]. It has been widely used in describing phenomena such as Benjamin-Feir-type modulational instabilities, solitons [27], and more recently, rogue waves [31,32]. Interestingly, the NLS equation can be derived by symmetry considerations alone [28]. However, for specific applications the coefficients of the various terms must be determined through a multiple-scale analysis procedure. Then, the NLS equation is obtained as a compatibility condition, imposed for secular term suppression, in third order in the small expansion parameter. The analogous first- and second-order compatibility conditions are also physically meaningful, as they yield the linear dispersion relation and the associated group velocity for the envelope. Higher-order compatibility conditions contribute additional nonlinear terms [33], which may lead to a nonintegrable perturbed NLS equation. In plasma physics, use of the cubic NLS equation has a long history, for example, to describe modulated electrostatic wavepackets [34] and weakly relativistic laser-plasma interactions [35–37]. For the case of linear polarization, in the highly under-dense plasma limit $\omega_{\rm pe}/\omega \ll 1$, fifth-order terms in the multiple scale expansion have been partially retained in Ref. [36]. The main contribution of the present paper is the derivation of the fifth-order terms for the overdense, near-critical case, with circular polarization.

This paper is structured as follows: Sec. II recalls the relativistic cold-fluid model that will be the starting point for this work. The multiple-scale expansion is described in Sec. III leading to the derivation of the pNLS equation, which is our main result. In Sec. IV we study in some detail the NLS equation limit of our expansion, comparing numerical results of cold-fluid model simulations to classical predictions of quasi-particle theory for soliton interaction. In Sec. V we compare numerical simulations of soliton interaction in the three levels of description: cold-fluid model, pNLS equation, and NLS equation. In Sec. VI we discuss our findings and present our conclusions. Appendix A describes the relation between fluid and envelope initial conditions, while Appendix B provides details on the numerical implementation of the fluid code.

II. RELATIVISTIC COLD FLUID MODEL

Our starting point is the relativistic cold-fluid plasma-Maxwell model (see, for example, Ref. [38] for the derivation and history of the model) in one spatial dimension. We assume a cold plasma of infinite extent with immobile ions that provide a neutralizing background. Considering infinite plane waves, propagating along the x direction and working in the Coulomb gauge, the longitudinal and transverse component of Ampere's law are expressed as

$$\frac{\partial^2\Phi}{\partial x\partial t}+\frac{N}{\gamma}P_x=0, \tag{1a}$$

and

$$\frac{\partial^2\mathbf{A}_\perp}{\partial x^2}-\frac{\partial^2\mathbf{A}_\perp}{\partial t^2}=\frac{N}{\gamma}\mathbf{A}_\perp, \tag{1b}$$

respectively. The fluid momentum equation is

$$\frac{\partial P_x}{\partial t}=\frac{\partial}{\partial x}(\Phi-\gamma), \tag{1c}$$

while Poisson equation yields

$$N=1+\frac{\partial^2\Phi}{\partial x^2}. \tag{1d}$$

Here,

$$\gamma=\sqrt{1+P_x^2+\mathbf{A}_\perp^2} \tag{1e}$$

is the relativistic factor, while $\mathbf{P}(x,t)=\mathbf{p}(x,t)-\mathbf{A}(x,t)$ is the generalized momentum of the electron fluid, $\mathbf{p}(x,t)$ is the kinetic momentum normalized to m_ec, N is the fluid charge density normalized to the plasma background density N_0, $\mathbf{A}_\perp=A_y\hat{\mathbf{j}}+A_z\hat{\mathbf{k}}$ is the transverse vector potential, and Φ is the scalar potential, both normalized to m_ec^2/e. Moreover, time and length are, respectively, normalized to the inverse of the plasma frequency $\omega_{\rm pe}$ and the corresponding skin depth $c/\omega_{\rm pe}$. In our one-dimensional modeling, we have taken the longitudinal vector potential $A_x=0$, while we have used the conservation of transverse canonical momentum, assuming an initially cold plasma, to write Eqs. (1b) and (1e).

III. MULTIPLE SCALE EXPANSION

Multiple scale analysis (see, e.g., Ref. [27]) seeks to describe perturbatively a system of differential equations by assuming it evolves in different, well-separated temporal and spatial scales. Our treatment follows the standard procedure of removal of secular terms by imposing suitable solvability conditions at each order in perturbation analysis. However, our treatment of the dispersion relation in Sec. III B is novel and has been devised in order to relate the electromagnetic field frequency to the small parameter of the expansion, while introducing localization of solutions in an overdense plasma in a natural way.

We proceed by introducing the scaled (or slow) variables $T_j=\epsilon^j t$ and $X_j=\epsilon^j x$, where ϵ is a small parameter and $j=0,1,2,\ldots$. We assume that the fields within the plasma are small, so that we may expand the fluid model variables as

$$A_y(x,t)=\sum_{j=1}^{\infty}\epsilon^j a_j(X_0,X_1,\ldots,T_0,T_1,\ldots), \tag{2a}$$

$$A_z(x,t)=\sum_{j=1}^{\infty}\epsilon^j b_j(X_0,X_1,\ldots,T_0,T_1,\ldots), \tag{2b}$$

$$\Phi(x,t) = \sum_{j=1}^{\infty} \epsilon^j \phi_j(X_1, \ldots, T_1, \ldots), \tag{2c}$$

$$P_x(x,t) = \sum_{j=1}^{\infty} \epsilon^j p_j(X_1, \ldots, T_1, \ldots), \tag{2d}$$

$$N(x,t) = \sum_{j=0}^{\infty} \epsilon^j n_j(X_1, \ldots, T_1, \ldots), \tag{2e}$$

and

$$\gamma = \sum_{j=0}^{\infty} \epsilon^j \gamma_j = 1 + \frac{1}{2}\left(p_1^2 + a_1^2 + b_1^2\right)\epsilon^2 + \ldots. \tag{2f}$$

Moreover, we will need

$$\delta \equiv 1/\gamma = \sum_{j=0}^{\infty} \epsilon^j \delta_j = 1 - \frac{1}{2}\left(p_1^2 + a_1^2 + b_1^2\right)\epsilon^2 + \ldots. \tag{2g}$$

In writing Eq. (2e) we took into account Eqs. (1d) and (2c). We assumed that the longitudinal quantities Φ, P_x, and N do not depend on the fast time scale T_0 associated with the transverse electromagnetic field oscillations, and took into account that for CP pulses there is no generation of harmonics of the basic frequency ω [4,35]. These assumptions are consistent with CP soliton solutions of Ref. [5], the interactions of which we shall study here.

Defining $\partial_i \equiv \partial/\partial T_i$ and $\nabla_i \equiv \partial/\partial X_i$, we get

$$\frac{\partial}{\partial t} = \partial_0 + \epsilon\partial_1 + \epsilon^2\partial_2 + \ldots, \tag{3a}$$

$$\frac{\partial}{\partial x} = \nabla_0 + \epsilon\nabla_1 + \epsilon^2\nabla_2 + \ldots, \tag{3b}$$

$$\frac{\partial^2}{\partial x\,\partial t} = \nabla_0\partial_0 + \epsilon(\nabla_0\partial_1 + \nabla_1\partial_0) + \ldots, \tag{3c}$$

etc.

We proceed by substituting Eq. (2) and Eq. (3) into Eq. (1), and collecting terms in different orders of ϵ.

A. Order ϵ^0

The only equation that contains terms of order ϵ^0 is Eq. (1d), which gives

$$n_0(X_0, X_1, \ldots, T_0, T_1, \ldots) = 1. \tag{4}$$

B. Order ϵ^1: linear dispersion relation

Collecting terms of order ϵ, Eqs. (1a)–(1c) give $p_1 = n_1 = 0$, while ϕ_1 remains unspecified. Taking into account Eq. (4), we get for the y component of Eq. (1b),

$$\nabla_0^2 a_1 - \partial_0^2 a_1 = a_1. \tag{5}$$

We are interested in plane wave solutions of this linear wave equation, which have the form

$$a_1(X_0, X_1, \ldots, T_0, T_1, \ldots) = a(X_1, \ldots, T_1, \ldots)e^{i(kX_0 - \omega T_0)} + \text{c.c.}, \tag{6}$$

where + c.c. denotes the complex conjugate of the preceding expression. Plugging Eq. (6) back into Eq. (5), we see that these solutions satisfy the usual plasma dispersion relation

$$\omega^2 = 1 + k^2. \tag{7}$$

Here, we are interested in overdense plasmas, in which $\omega < 1$ and thus

$$k^2 = \omega^2 - 1 < 0, \tag{8}$$

i.e., k is imaginary and the waves are localized. Moreover, we are interested here in describing solutions close to small amplitude solitons, which have $\omega \simeq 1$. Therefore, $|k|$ is small and this fact in combination with the dispersion relation, Eq. (7), suggests the following expansions,

$$\omega = \sum_{j=0}^{\infty} \epsilon^j \omega_j, \qquad k = \sum_{j=1}^{\infty} \epsilon^j k_j. \tag{9}$$

Substituting Eq. (9) into the dispersion relation Eq. (7), we obtain

$$\omega = 1 - \frac{\epsilon^2}{2}|k_1|^2 + \ldots, \tag{10}$$

where we used $k_1 = \pm i|k_1|$. This implies that expressions such as $\epsilon|k_1|\,X_0$, $\epsilon^2|k_1|^2 T_0$, etc. appearing in the oscillating part of Eq. (6), do in fact represent slow variations. Thus, we may include them into the envelope, i.e., we may write Eq. (6) as

$$a_1(X_0, X_1, \ldots, T_0, T_1, \ldots) = a(X_1, \ldots, T_1, \ldots)e^{-iT_0} + \text{c.c.} \tag{11}$$

Note that the dependence on X_0 has naturally dropped.

C. Order ϵ^2

Collecting terms of order ϵ^2 we get from Eqs. (1a) and (1d) $p_2 = n_2 = 0$, while Eq. (1c) yields

$$\nabla_1\phi_1 - \tfrac{1}{2}\nabla_0\left(a_1^2 + b_1^2\right) = 0, \tag{12}$$

respectively. For circular polarization (CP), we have $a = -i\,b$, and therefore Eq. (2f) yields

$$\gamma_2 = \tfrac{1}{2}\left(a_1^2 + b_1^2\right) = 2\,|a|^2, \tag{13}$$

independent of T_0. Thus, Eq. (12) simplifies to

$$\nabla_1\phi_1 = 0. \tag{14}$$

Collecting terms of order ϵ^2 we get for the y component of Eq. (1b),

$$\mathcal{L}a_2 = 2\partial_0\partial_1 a_1 = -2\,i\,\frac{\partial a}{\partial T_1}e^{-iT_0}, \tag{15}$$

where we introduced the operator

$$\mathcal{L} \equiv \left(\nabla_0^2 - \partial_0^2 - 1\right). \tag{16}$$

The term on the right-hand side is a resonant forcing term for the linear operator $\mathcal{L}$. Therefore, we impose the solvability condition

$$\frac{\partial a}{\partial T_1} = 0. \tag{17}$$

Then Eq. (15) becomes $\mathcal{L}a_2 = 0$. It has plane wave solutions that can be included in a_1 in Eq. (11), so we may take $a_2 = 0$. From Eq. (2f) we then find $\gamma_3 = 0$.

D. Order ϵ^3: NLS equation limit

Collecting terms of order ϵ^2 and using Eq. (14), we get from Eqs. (1a)–(1c), $p_3 = n_3 = 0$, and

$$\nabla_2\phi_1 + \nabla_1(\phi_2 - 2|a|^2) = 0, \tag{18}$$

respectively. Operating on Eq. (18) with ∇_1 and using Eq. (14), we obtain

$$\nabla_1^2(\phi_2 - 2|a|^2) = 0, \tag{19}$$

which, requiring that ϕ_2 and a vanish as $X_1 \to \infty$, implies

$$\nabla_1(\phi_2 - 2|a|^2) = 0. \tag{20}$$

Then in turn, Eq. (18) implies

$$\nabla_2\phi_1 = 0. \tag{21}$$

Collecting terms of order ϵ^2 we get for the y component of Eq. (1b),

$$\mathcal{L}a_3 = -\nabla_1^2 a_1 + \left(\partial_1^2 + 2\partial_0\partial_2\right)a_1 - 2|a|^2 a_1, \tag{22}$$

$$= -\frac{\partial^2 a}{\partial X_1^2}e^{-iT_0} - 2\,i\,\frac{\partial a}{\partial T_2}e^{-iT_0} - 2\,|a|^2 a\,e^{-iT_0}, \tag{23}$$

where we also used Eq. (17). The terms in the right-hand side are all resonant with the operator $\mathcal{L}$, leading to the solvability condition

$$i\,\frac{\partial a}{\partial T_2} + \frac{1}{2}\frac{\partial^2 a}{\partial X_1^2} + |a|^2 a = 0. \tag{24}$$

This is a NLS equation. Imposing the solvability condition Eq. (24), we get from Eq. (22), $\mathcal{L}a_3 = 0$, or $a_3 = 0$.

According to the standard multiple scale treatment of waves in the fluid plasma description, the cubic NLS equation, Eq. (24), is obtained at this order, and the iterative expansion procedure stops here. An exception is Ref. [36], where the limit of small density ($\omega_{pe} \ll \omega$) has been considered and a different scaling of the slow variables has been derived, partially including terms of fifth order in ϵ. The absence of harmonic terms for circular polarization makes the ϵ expansion much simpler in our case and allows us to keep all terms up to fifth order in the following, deriving a single perturbed NLS equation.

E. Order ϵ^4

From Eq. (1a) we get, with the help of Eqs. (14) and (21),

$$\nabla_1\partial_1\phi_2 + p_4 = 0. \tag{25}$$

Operating with ∂_1 on Eq. (20) and using Eq. (17) we obtain

$$\nabla_1\partial_1\phi_2 = 0, \tag{26}$$

and therefore $p_4 = 0$.

Equation (1d) gives

$$n_4 = \nabla_1^2\phi_2. \tag{27}$$

Noting that

$$\gamma_4 = -2\,|a|^4, \tag{28}$$

we get from Eq. (1c)

$$\nabla_1\phi_3 + \nabla_3\phi_1 + \nabla_2(\phi_2 + 2|a|^2) = 0. \tag{29}$$

Collecting terms of order ϵ^4 we get for the y component of Eq. (1b),

$$\mathcal{L}a_4 = 2\partial_0\partial_3 a_1 - 2\nabla_1\nabla_2 a_1 \tag{30}$$

$$= -2\,i\,\partial_3 a\,e^{-iT_0} - 2\nabla_1\nabla_2 a\,e^{-iT_0}. \tag{31}$$

Requiring that resonant forcing terms vanish, we obtain the solvability condition

$$i\,\partial_3 a + \nabla_1\nabla_2 a = 0. \tag{32}$$

Finally, Eq. (30) implies a_4 may be included into a_1 and we write $a_4 = 0$.

F. Order ϵ^5

Equation (1a) gives

$$p_5 + \nabla_3\partial_1\phi_1 + \nabla_2\partial_1\phi_2 + \nabla_1\partial_2\phi_2 + \nabla_1\partial_1\phi_3 = 0, \tag{33}$$

where we have used Eqs. (21) and (14). Applying ∇_1 on Eq. (29) and using Eqs. (14) and (20), we get

$$\nabla_1^2\phi_3 = 0, \tag{34}$$

which implies

$$\nabla_1\phi_3 = 0. \tag{35}$$

On the other hand, applying ∂_1 on Eq. (29) and using Eqs. (17) and (35), we get

$$\nabla_3\partial_1\phi_1 + \nabla_2\partial_1\phi_2 = 0. \tag{36}$$

Thus, we may use Eqs. (35)–(36) to get from Eq. (33)

$$p_5 = -\nabla_1\partial_2\phi_2 = -2\partial_2\nabla_1|a|^2, \tag{37}$$

where, in the last step, we have used Eq. (20).

From the Poisson equation, Eq. (1d), we obtain

$$n_5 = 2\nabla_2\nabla_1\phi_2 = 4\nabla_2\nabla_1|a|^2. \tag{38}$$

Equation (1c) gives

$$\nabla_1(\phi_4 - \gamma_4) + \nabla_2\phi_3 + \nabla_3(\phi_2 - \gamma_2) + \nabla_4\phi_1 = 0. \tag{39}$$

Operating on Eq. (39) with ∇_1 and using Eqs. (20), (19), and (35), we obtain

$$\nabla_1^2(\phi_4 - \gamma_4) = 0. \tag{40}$$

Noting that $\delta_4 = 6\,|a|^4$, the wave equation gives at order ϵ^5

$$\mathcal{L}\,a_5 = -2\nabla_1\nabla_3 a_1 - \nabla_2^2 a_1 + 2\partial_0\partial_4 a_1 + \partial_2^2 a_1 + 6|a|^4 a_1 + n_4 a_1. \tag{41}$$

All terms on the right-hand side are resonant forcing terms, and with the help of Eqs. (27) and (19), we are led to the solvability condition

$$-2\nabla_1\nabla_3 a - \nabla_2^2 a - 2\,i\,\partial_4 a + \partial_2^2 a + 6|a|^4 a + 2a\nabla_1^2|a|^2 = 0. \tag{42}$$

We note that we do not employ a parabolic approximation but rather maintain the term involving second-time derivative. Finally, Eq. (41) allows one to write $a_5 = 0$.

G. Collecting different orders: pNLS equation

The strategy we follow in order to write a perturbed NLS equation, inspired by Ref. [33] (Chapter 3), is to multiply the solvability conditions imposed at various orders with appropriate constants, so as to form the expansions of the differential operators Eq. (3). Specifically, we form the sum

$$2\,i\,\epsilon\times(17)+2\,\epsilon^2\times(24)+2\,\epsilon^3\times(32)-\epsilon^4\times(42), \quad (43)$$

which, using Eq. (3), reads

$$i\frac{\partial a}{\partial t}+\frac{1}{2}\frac{\partial^2 a}{\partial x^2}+\epsilon^2|a|a-3\,\epsilon^4|a|^4a-\epsilon^2\frac{\partial^2|a|^2}{\partial x^2}a-\frac{1}{2}\frac{\partial^2 a}{\partial t^2}=0. \quad (44)$$

Rescaling,

$$X=\epsilon x, \qquad T=\epsilon^2 t, \quad (45)$$

we arrive at

$$i\frac{\partial a}{\partial T}+\frac{1}{2}\frac{\partial^2 a}{\partial X^2}+|a|^2a=\epsilon^2\left(3\,|a|^4a+\frac{\partial^2|a|^2}{\partial X^2}a+\frac{1}{2}\frac{\partial^2 a}{\partial T^2}\right), \quad (46)$$

which is our main result. Equation (46) has the form of a singularly perturbed nonlinear Schrödinger equation, since the highest-order time derivative appears in the perturbation term. Note that, due to our treatment of the dispersion relation in Sec. III B, Eq. (46) is written in the laboratory frame, without the need of a coordinate transformation to a frame moving with the group velocity $v_g=\omega'(k)$, which is usually required in the derivation of NLS-type equations. We therefore bypass any problems related to the fact that $\omega'(k)$ as obtained from Eq. (7) is imaginary.

Solution of Eq. (46) for $a(X,T)$ also determines the rest of the variables in the perturbation expansion of the cold-fluid model. Indeed, we get from Eqs. (2e), (4), (27), and (38), in a similar manner as above,

$$N=1+2\,\epsilon^4\frac{\partial^2|a|^2}{\partial X^2}+\mathcal{O}(\epsilon^6), \quad (47)$$

i.e., n_5 may be included in the fourth order terms.

Similarly, Eq. (37) gives

$$P=-2\,\epsilon^5\frac{\partial^2|a|^2}{\partial T\,\partial X}+\mathcal{O}(\epsilon^6). \quad (48)$$

Finally, noting that Eq. (14) yields

$$\nabla_1^2\phi_1=0, \quad (49)$$

and forming the sum

$$\epsilon\times(49)+\epsilon^2\times(19)+\epsilon^3\times(34)+\epsilon^4\times(40), \quad (50)$$

we obtain

$$\frac{\partial^2}{\partial X^2}(\Phi-\gamma)=\mathcal{O}(\epsilon^5). \quad (51)$$

Noting that Φ,γ, do not depend on X_0, and taking into account boundary conditions at $x\to\pm\infty$, we obtain

$$\Phi=\gamma-1+\mathcal{O}(\epsilon^5) \quad (52)$$

$$=2|a|^2\,\epsilon^2-2|a|^4\,\epsilon^4+\mathcal{O}(\epsilon^5). \quad (53)$$

Therefore, the solution of Eq. (46) for $a(X,T)$, also determines N, P, and Φ.

The cubic $|a|^2a$ and quintic terms $3\,\epsilon^2|a|^4a$ come from the expansion of the relativistic factor γ and therefore correspond to relativistic corrections to the optical properties of the plasma, i.e., they pertain to transverse dynamics. The cubic term results in compression of the pulse, while the quintic term has the opposite effect (due to the difference in sign). The term $a\,\partial_{XX}|a|^2$ takes into account longitudinal effects, namely the coupling of the electromagnetic field to the plasma through charge separation caused by ponderomotive effects [see Eq. (47)]. Moreover, Eq. (48) shows that the balance of ponderomotive $\partial_X\gamma$ and electrostatic force $\partial_X\phi$ implied by Eq. (51), is violated at order ϵ^5 [see also Eq. (1c)].

IV. NLS EQUATION LIMIT

Neglecting terms of order ϵ^2, Eq. (46) reduces to a NLS equation [39],

$$i\,\frac{\partial a}{\partial T}+\frac{1}{2}\frac{\partial^2 a}{\partial X^2}+|a|^2a=0, \quad (54)$$

which has both moving and standing envelope soliton solutions, which we now briefly study in order to establish connection with cold-fluid model solitons.

A. Moving soliton solutions

Moving soliton solutions of Eq. (54) have the form [27]

$$a(X,T)=\alpha_0\,\mathrm{sech}\,[\alpha_0(X-u_e\,T)]\,e^{i\,u_e\,(X-u_p\,T)}, \quad (55)$$

where u_e is the envelope (or group) velocity, u_p is the phase velocity, and the amplitude a_0 is given by

$$\alpha_0=\sqrt{u_e^2-2\,u_e\,u_p}. \quad (56)$$

Note that u_e and u_p refer to the scaled variables X and T. We can go back to the original variables by using Eq. (A1) of Appendix A, which gives

$$A_y=F_0(x,t)\,\cos[u_e\epsilon x-(1+u_eu_p\epsilon^2)t], \quad (57)$$

where $F_0(x,t)=2\,\alpha\,\epsilon\,\mathrm{sech}\,[\alpha_0\epsilon\,(x-\epsilon u_e t)]$. A similar expression can be written for A_z, while Eqs. (47), (48), and (52) provide expressions for the remaining fluid variables. We see that the phase and group velocity read

$$v_{\mathrm{ph}}=\frac{1+u_eu_p\epsilon^2}{u_e\epsilon}, \quad (58)$$

and

$$v_g=\epsilon u_e, \quad (59)$$

respectively. Therefore, in terms of the cold-fluid model, moving soliton solutions Eq. (55) represent slowly propagating solitons.

We show an example of propagating NLS equation solitons Eq. (55) with $u_e=0.9$, $u_p=0.1$, and $\epsilon=0.141$ in Fig. 1. Although this is only an approximate soliton solution of the pNLS equation and cold-fluid model, we observe propagation at the predicted group velocity ϵu_e, while the solution approximately maintains its shape. An exact propagating soliton solution would have to be determined by methods similar to those used, for example, in Refs. [4,21]. This is, however,

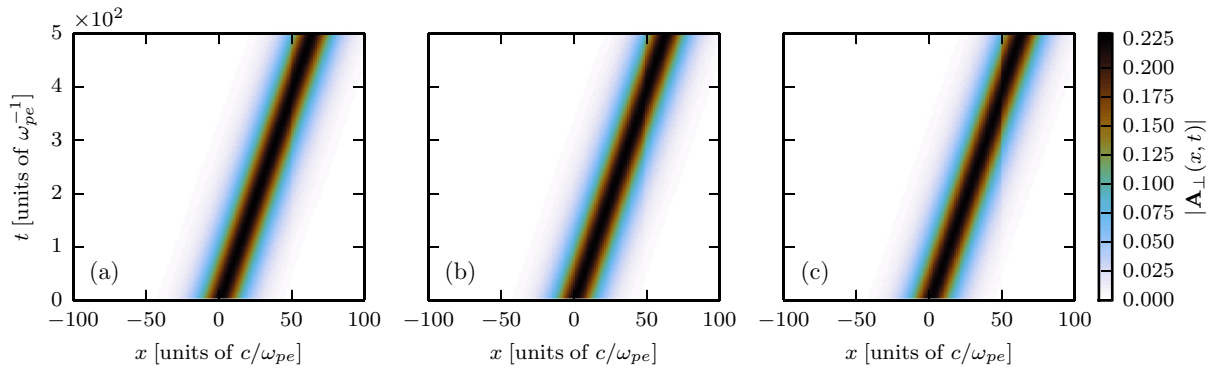

FIG. 1. (Color online) Simulation of a propagating soliton with $u_e = 0.9$, $u_p = 0.1$, and $\epsilon = 0.141$, using (a) the fluid model Eq. (1), (b) pNLS Eq. (46), and (c) NLS Eq. (24).

outside the scope of this work, which emphasizes standing soliton interactions.

B. Standing soliton solutions

Standing soliton solutions of Eq. (54) have the form

$$a(X,T) = \phi(X)e^{-i\lambda T}, \tag{60}$$

where the frequency λ is to be determined. A well-known soliton family of Eq. (54) has the form (see, e.g., Ref. [27])

$$\phi(X,T) = \alpha\,\mathrm{sech}[\alpha(X - X_0)], \tag{61}$$

where the amplitude α is constant. Substituting Eqs. (60) and (61) into Eq. (54), we obtain

$$\lambda = -\tfrac{1}{2}\alpha^2. \tag{62}$$

Using Eq. (A1) of Appendix A, one may go back to the original cold-fluid model variables,

$$A_y(x,t) = C_0(x)\,\cos(t - \epsilon^2\alpha^2\,t/2), \tag{63a}$$

$$A_z(x,t) = C_0(x)\,\sin(t - \epsilon^2\alpha^2\,t/2), \tag{63b}$$

where $C_0(x) = 2\epsilon\alpha\,\mathrm{sech}[\epsilon\alpha(x - x_0)]$. Note that the term $-\epsilon^2\alpha^2\,t/2$ corresponds to the term $-\epsilon^2|k_1|^2\,t/2$ in Eq. (10), which has been included into the envelope. This correction to ω, therefore, corresponds to slow oscillations of the soliton envelope, and we may identify $\alpha = |k_1|$.

A connection to exact cold-fluid mode solitons of Esirkepov *et al.* [5], which have

$$A_y = R(x)\,\cos(\omega t), \qquad A_z = R(x)\,\sin(\omega t), \tag{64}$$

where

$$R(x) = \frac{2\sqrt{1-\omega^2}\,\cosh[\sqrt{1-\omega^2}(x - x_0)]}{\cosh^2[\sqrt{1-\omega^2}(x - x_0)] + \omega^2 - 1}, \tag{65}$$

can now be established. Taking into account that Eq. (10) yields

$$\omega^2 = 1 - \epsilon^2\,|k_1|^2, \tag{66}$$

A_y from Eq. (64) becomes, in leading order in ϵ,

$$A_y = 2\epsilon|k_1|\,\mathrm{sech}\,[\epsilon|k_1|(x - x_0)]\,\cos(t - \epsilon^2\,|k_1|^2\,t/2). \tag{67}$$

Comparison of Eq. (63a) with Eq. (67), once again shows that we may identify $\alpha = |k_1|$. The value of $|k_1|$ still remains unspecified, apart from the requirement that $|k_1| \sim \mathcal{O}(1)$, which follows from Eq. (9). For the study of a single soliton, or interacting solitons of the same amplitude, we may, without loss of generality, set $|k_1| = 1$, i.e., work with $\alpha = 1$ in Eq. (63). Then, the small parameter ϵ in the expansion is related to ω through

$$\epsilon = \sqrt{1 - \omega^2}. \tag{68}$$

However, the indeterminancy of k_1 in Eq. (67) allows us to model interactions of solitons with different frequencies (and therefore amplitudes) using a single small parameter ϵ; see Sec. V.

C. Quasiparticle approach to soliton interactions

Soliton interactions of NLS Eq. (54) have been studied through different methods and are well understood, particularly when the separation of the two solitons is large; see, for example, Ref. [25]. In that case, one may consider the solitons as "quasiparticles," i.e., independent entities that exert a force to one another and to a good approximation maintain their shape during their interaction [25,40,41] (adiabatic approximation). One then may approximate the evolution of the solitons with a set of few coupled ordinary differential equations for the evolution of the soliton parameters.

A particularly useful perspective is that of Gordon [41], who shows that within this framework the dynamics of two solitons may be described by the system of ODEs,

$$\ddot{D} = -8\,e^{-D}\,\cos(\Psi), \tag{69a}$$

$$\ddot{\Psi} = 8\,e^{-D}\,\sin(\Psi), \tag{69b}$$

where $D(T)$ and $\Psi(T)$ are the soliton peak-to-peak distance and relative phase, respectively, $1 \pm \dot{\Psi}/2$ are their amplitudes, and a dot indicates derivative with respect to T. Therefore, the solitons exert to each other an effective force with magnitude that decreases exponentially with distance D and a sign that depends on their relative phase Ψ.

For the particular case of solitons of equal initial amplitude, $\dot{\Psi}_0 = 0$, and zero initial phase difference, we see from Eq. (69) that the force is attractive, while the relative phase remains zero, leading to the formation of an oscillatory bound state. A detailed calculation [25,41] shows that the peak-to-peak

separation varies as

$$D(T) = D_0 + 2\ln|\cos(2\,e^{-D_0/2}\,T)|, \tag{70}$$

where $D_0 \gg 1$ is the initial distance. Equation (70) implies that the time after which the solitons collide for the first time is [25,41]

$$T_{\rm coll} = \frac{1}{2}e^{D_0/2}\cos^{-1}(e^{-D_0/2}) \simeq \frac{\pi}{4}e^{D_0/2}. \tag{71}$$

We note that in scaled variables collision time $T_{\rm coll}$ is, according to Eq. (71), independent of ω. However, when we go back to units of $\omega_{\rm pe}^{-1}$ and $c/\omega_{\rm pe}$ for time and space, respectively, through Eqs. (45) and (68), we obtain

$$t_{\rm coll} = \frac{\pi}{4(1-\omega^2)}e^{\sqrt{(1-\omega^2)}\,d_0/2}, \tag{72}$$

where $t_{\rm coll} = T_{\rm coll}/\epsilon^2$ and $d_0 = D_0/\epsilon$. For large enough d_0, $t_{\rm coll}$ decreases for increasing ω. Analytical predictions of Eq. (72) are compared with numerical simulations in Sec. V.

For solitons of equal initial amplitude, $\dot\Psi_0 = 0$, and initial relative phase Ψ_0, the separation versus time reads [25]

$$D(T) = D_0 + \ln\left|\frac{\cosh(-\kappa_1\,T) + \cos(\kappa_2\,T)}{2}\right|, \tag{73}$$

where

$$\kappa_1 = 4\,e^{-D_0/2}\,\sin(\Psi_0/2)\,, \qquad \kappa_2 = 4\,e^{-D_0/2}\cos(\Psi_0/2)\,.$$

Thus, the solitons eventually drift apart since, as we see from Eq. (69), the force is not attractive for all T. For large T, after the solitons drift apart, the soliton amplitudes differ by

$$|\Delta a| = |a_1 - a_2| = |4\,e^{-D_0/2}\cos(\Psi_0/2)\,|. \tag{74}$$

The minimum peak-to-peak distance is

$$D_{\rm min} = D_0 + \ln\left\{\frac{1}{2}\left[\cosh\left(-\pi\tan\frac{\Psi_0}{2}\right) - 1\right]\right\} \tag{75}$$

reached at time

$$T_{\rm min} = \frac{\pi}{4\cos(\Psi_0/2)}e^{D_0/2} \tag{76}$$

or, in units of $\omega_{\rm pe}^{-1}$,

$$t_{\rm min} = \frac{\pi\,e^{\sqrt{(1-\omega^2)}\,d_0/2}}{4(1-\omega^2)\cos(\Psi_0/2)}. \tag{77}$$

From Eq. (75) one finds [25] that the collision is inhibited for initial phase $\Psi_0 > \Psi_c$, where

$$\tan\frac{\Psi_c}{2} = \frac{1}{\pi}\cosh^{-1}(1 + 2\,e^{-D_0}). \tag{78}$$

In the case of solitons with different initial amplitudes, $\dot\Psi_0 \neq 0$, and no initial relative phase, $\Psi_0 = 0$, one finds that the solitons form an oscillatory bound state, with their distance oscillating periodically between a minimum and a maximum distance. Qualitative results can also be obtained for this case and may be found in Ref. [25].

V. NUMERICAL SIMULATIONS

This section compares numerical simulations of soliton interactions of the three different levels of description: the cold-fluid model Eq. (1), the pNLS equation Eq. (46), and the NLS equation (24). Where appropriate, comparisons of the simulation results and the quasiparticle predictions of Sec. IV C are also presented.

We investigate the interactions of standing solitons first found by Esirkepov *et al.* [5]. Labeling each soliton by an index (j), we have for the cold-fluid model variables

$$A_y^{(j)}(x,t) = \frac{2\sqrt{1-\omega_j^2}\cosh^2(\zeta_j)}{\cosh^2(\zeta_j)+\omega_j^2-1}\cos(\omega_j\,t+\theta_j),$$

$$A_z^{(j)}(x,t) = \frac{2\sqrt{1-\omega_j^2}\cosh^2(\zeta_j)}{\cosh^2(\zeta_j)+\omega_j^2-1}\sin(\omega_j\,t+\theta_j), \tag{79a}$$

$$E_x^{(j)}(x,t) = \frac{4\left(1-\omega_j^2\right)^{3/2}\cosh(\zeta_j)\sinh(\zeta_j)}{\left(\cosh^2(\zeta_j)+\omega_j^2-1\right)^2},$$

$$E_y^{(j)}(x,t) = \omega_j\,A_z^{(j)}\,, \quad E_z^{(j)} = -\omega_j\,A_y^{(j)}, \tag{79b}$$

$$N^{(j)}(x,t) = 1 + \left(1-\omega_j^2\right)^2 \times \frac{\cosh(4\zeta_j) - 2\,(2\,\omega_j^2-1)\,\cosh(2\,\zeta_j) - 3}{\left(\cosh^2(\zeta_j)-1+\omega_j^2\right)^3},$$

$$P_x = 0, \tag{79c}$$

where $\zeta_j = \sqrt{1-\omega_j^2}(x-x_j)$ and θ_j is an initial phase. The soliton amplitude is $R_0^{(j)} \equiv |\mathbf{A}_\perp(x_j)| = 2\sqrt{1-\omega^2}/\omega^2$. It takes its maximum value $R_{0,\rm max} = \sqrt{3}$ for $\omega_{\rm min} = \sqrt{2/3}$, where the branch of Esirkepov solitons terminates because the minimum local density vanishes.

In the following, we study interactions of pairs of solitons with frequencies ω_1, ω_2 and initial phase difference $\Psi_0 = \theta_2 - \theta_1$, i.e., with initial conditions given by $A_y(x,0) = A_y^{(1)}(x,0) + A_y^{(2)}(x,0)$, etc. For the density we take care that the boundary condition $N(x,0) \to 1$ as $x \to \pm\infty$ is satisfied by using the initial condition $N(x,0) = N^{(1)}(x,0) + N^{(2)}(x,0) - 1$.

For the simulations using pNLS Eq. (46), we introduce a parameter $k_1^{(j)}$ for each soliton. We then set $|k_1^{(1)}| = 1$, which fixes $\epsilon = \sqrt{1-\omega_1^2}$ through Eq. (66), and introduce the soliton amplitude as $\alpha_j = \sqrt{1-\omega_j^2}/\epsilon$, effectively using the freedom to choose $k_1^{(j)} = \alpha_j$. Then, according to Eqs. (A3) and (A5) of Appendix A, initial conditions for the soliton centered at $x_j = X_j/\epsilon$ are given as

$$a^{(j)}(X,0) = \frac{\alpha_j\cosh^2[\alpha_j(X-X_j)]}{\cosh^2[\alpha_j(X-X_j)]+\omega_j^2-1}\,e^{-i\theta_j}, \tag{80a}$$

$$\left.\frac{\partial a^{(j)}}{\partial T}\right|_{T=0} = \frac{i\,\alpha_j^2}{2}\,a^{(j)}(X,0). \tag{80b}$$

Finally, for the simulations with the NLS equation Eq. (54), we expand Eq. (80a) to lowest order in ϵ, to obtain the NLS equation soliton

$$a^{(j)}(X,0) = \alpha_j\,\mathrm{sech}[\alpha_j(X-X_j)]\,e^{-i\theta_j}. \tag{81}$$

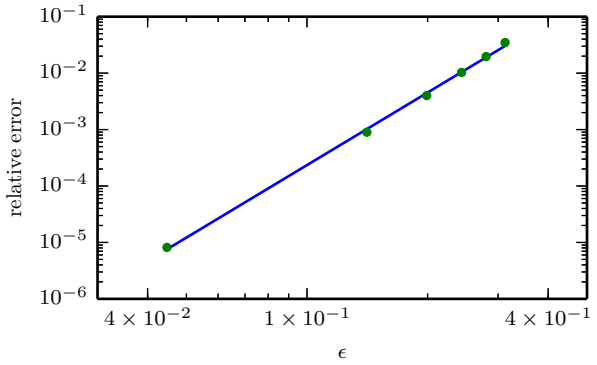

FIG. 2. (Color online) Estimate of the relative error introduced by neglecting higher-order terms in pNLS Eq. (46). We plot $\max\left[a(x,T) - a(x,0)\right]/a(0,0)$ for solutions of Eq. (46) up to $T/\epsilon^2 = 2 \times 10^4$, with initial condition Eq. (80) with $x_1 = 0$. Dots correspond to $\omega = (0.999, 0.99, 0.98, 0.97, 0.96, 0.95)$. The solid line is the best fit to the data, showing that rel. error $\sim \epsilon^{4.3}$.

All simulations are carried out with the package XMDS2 [42], using the pseudospectral method with Fourier space evaluation of partial derivatives and a fourth-order adaptive Runge-Kutta-Fehlberg scheme (known as ARK45) for time-stepping. More details on the implementation are provided in Appendix B. We validated our fluid code by verifying that a single soliton with $\omega_1 = 0.98$, i.e., of the largest amplitude $R_0^{(j)} = 0.414$ studied here, follows Eq. (79) up to $t = 2 \times 10^4$.

Initial conditions, Eq. (80), do not correspond to an exact soliton solution of the pNLS equation. However, by integrating such initial conditions up to $t = T/\epsilon^2 = 2 \times 10^4$, we show in Fig. 2 that the relative error introduced by the choice of initial conditions remains small for the maximum amplitude considered in the following numerical examples (corresponding to $\omega \geqslant 0.98$).

A. Small-amplitude limit

For small-amplitude solitons we find excellent agreement between cubic NLS equation, pNLS equation, and cold-fluid model predictions.

1. Solitary waves of equal amplitude and no phase difference

A typical case in which we have formation of a bound state of solitons is shown in Fig. 3. In these simulations, both solitons have frequencies $\omega_1 = \omega_2 = 0.999$, $R_0^{(1)} = R_0^{(2)} \simeq 0.0896$ (corresponding to $\epsilon \simeq 0.0447$, $k_1^{(1)} = k_1^{(2)} = 1$), initial distance is $d_0 = 100$, and there is no initial phase difference. The behavior of the exact cold-fluid model solutions is captured correctly by both the NLS and pNLS equation models. Therefore, at very small amplitudes, the behavior may be completely understood in terms of the NLS equation. The major role in soliton attraction and in bound-state formation is thus played by the leading term of the relativistic nonlinearity, i.e., by the cubic term in the NLS equation.

The predictions of quasiparticle theory of Sec. IV C for the collision time $t_{\rm coll}$ or the period of oscillations $t_p = 2\,t_{\rm coll}$ are in excellent agreement with fluid model simulations; see Fig. 4.

2. Solitary waves of equal amplitude and finite phase difference

Next, we study the case of two solitons of equal frequency $\omega_1 = \omega_2 = 0.999$ and amplitude $R_0^{(1)} = R_0^{(2)} \simeq 0.0896$ (corresponding to $\epsilon \simeq 0.0447$, $k_1^{(1)} = k_1^{(2)} = 1$) and a finite initial phase difference $\Psi_0 = 0.1\pi$; see Fig. 5. Also in this case, we find excellent quantitative agreement between cold-fluid model, NLS equation, and pNLS equation simulations. The solitons attract but do not collide, in agreement with quasiparticle theory, which predicts that collisions are inhibited for $\Psi_0 > \Psi_c = 0.136$. The solitons reach a minimum distance $d_{\rm min} \simeq 57$ at time $t_{\rm min} \simeq 3485$ and subsequently drift apart. Quasiparticle theory underestimates the minimum distance $d_{\rm min} = 38.2$, while the time of minimum approach $t_{\rm min} = 3720$ is in good agreement with simulations. According to quasiparticle theory, Eq. (74), the solitons differ in amplitude by $|\Delta A| = 2\,\epsilon\,|\Delta a| = 0.037$. This is in excellent agreement with the NLS simulation, for which the soliton amplitudes differ at $t = 10^5$ by $|\Delta A| = 0.036$.

3. Solitary waves of unequal amplitude and no phase difference

For solitons of unequal frequences $\omega_1 = 0.999$ and $\omega_2 = 0.998$, and therefore also unequal amplitudes $R_0^{(1)} \simeq 0.0896$, $R_0^{(2)} \simeq 0.127$ (corresponding to $\epsilon \simeq 0.0447$, $k_1^{(1)} = 1$, $k_1^{(2)} \simeq 1.4139$), with no initial phase difference, as shown in Fig. 6,

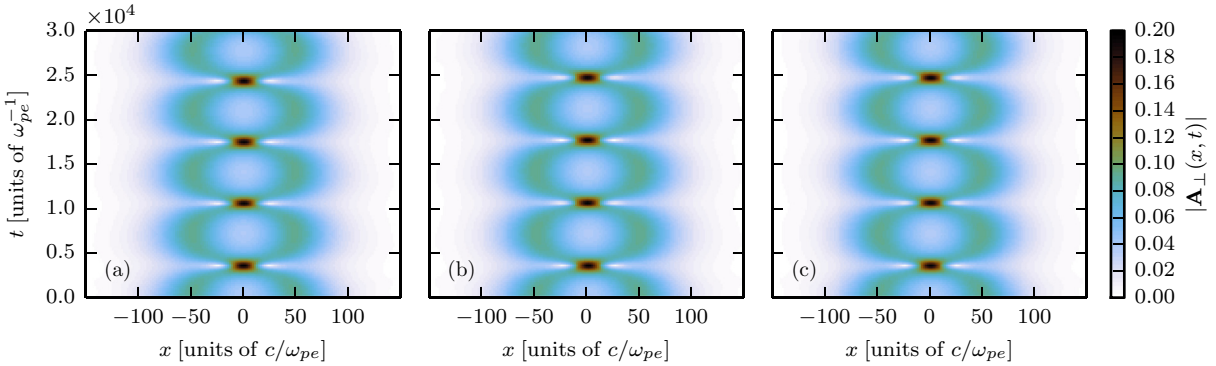

FIG. 3. (Color online) Comparison of simulations of two-soliton interaction with frequencies $\omega_1 = \omega_2 = 0.999$, $R_0^{(1)} = R_0^{(2)} \simeq 0.0896$ (corresponding to $\epsilon \simeq 0.0447$, $k_1^{(1)} = k_1^{(2)} = 1$) and initial distance $d_0 = 100$ using (a) the fluid model Eq. (1), (b) pNLS Eq. (46), and (c) NLS Eq. (24).

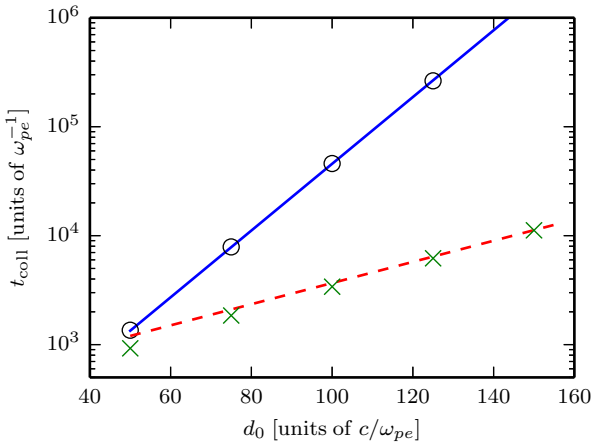

FIG. 4. (Color online) Comparison of results of quasiparticle theory for $\omega = 0.999$ (red, dashed line) and $\omega = 0.99$ (blue, solid line) with numerical results from simulations of the fluid model (circles and cross signs, respectively) for the first collision time $t_{\rm coll}$ for solitons of equal amplitude and no initial phase difference, as a function of initial separation d_0.

the solitons interact and form a periodic bound state. However, their separation remains finite. Again, there is excellent agreement between all three levels of description. This behavior can be also understood in terms of quasiparticle theory of NLS equation; see Ref. [25].

B. Larger amplitudes

For solitons of moderately large amplitude, but still in the perturbative regime $\epsilon \ll 1$, cold-fluid model simulations deviate from cubic NLS equation predictions and the fifth-order terms need to be taken into account.

1. *Solitary waves of equal amplitude and no phase difference*

Figure 7 shows the interaction of two solitons of equal amplitude with $\omega_1 = \omega_2 = 0.99$ ($R_{0,1} = R_{0,2} \simeq 0.2879$, $\epsilon \simeq 0.1411$, $k_1^{(1)} = k_1^{(2)} = 1$), separated by $d_0 = 60$, and no initial phase difference. The solitons collide approximately at $t_{\rm coll} \simeq 2800$, in good agreement with quasiparticle theory prediction $t_{\rm coll} \simeq 2717$, and they form a bound state. However, contrary to the prediction of the cubic NLS equation model, collisions are inelastic and part of the soliton field decays away each time the solitons collide; see Fig. 8. The bound state is reminiscent of a system of damped oscillators: after each encounter, the solitons decrease in amplitude and come closer together. In turn, this implies that the period of bound-state oscillations becomes shorter, as predicted by Eq. (72).

This behavior is also captured qualitatively by the pNLS equation; see Fig. 7(b). However, the pNLS equation overestimates the loss of soliton field at collisions and, correspondingly, the period of oscillations decreases with a faster rate than in the fluid model simulations. These deviations may be attributed to the breakdown, at the moment of collision, of the assumptions of small-field magnitude and slow spatiotemporal evolution. In particular, close to the collision, the spatial scale for variations in the envelope is a few $c/\omega_{\rm pe}$, indicating that we should expect quantitative discrepancies between the fluid and pNLS equation simulations.

The cubic NLS equation approximation on the other hand, presents qualitative difference in this case. Since cubic NLS equation is an integrable model, all soliton collisions are elastic, leading to an exactly periodic bound state of solitons. Therefore, the inclusion of the fifth-order terms in our analysis is necessary for a qualitatively correct description of soliton interactions.

The collision time on the other hand, as predicted by quasiparticle theory of NLS equation, agrees very well with fluid simulation results even in this larger amplitude case; see Fig. 4. The reason for this is that attraction of solitons is determined by their overlap. For large initial separation of the solitons, this overlap occurs at small amplitudes. Moreover, in the limit $x \to \pm\infty$ the exact soliton envelope Eq. (80a) takes the form of the NLS equation soliton Eq. (80b). Therefore, NLS equation approximation is a valid one in order to determine the initial attraction phase of two well-separated solitons, even for larger amplitudes.

2. *Solitary waves of equal amplitude and finite phase difference*

As an example, we show the interaction of two solitons with $\omega_1 = \omega_2 = 0.99$ ($R_{0,1} = R_{0,2} \simeq 0.2879$, $\epsilon \simeq 0.1411$, $k_1^{(1)} = k_1^{(2)} = 1$) with initial distance $d_0 = 60$ and phase difference $\Psi_0 = 0.1\,\pi$, in Fig. 9. The fluid simulations show that the solitons initially approach and then separate, moving in

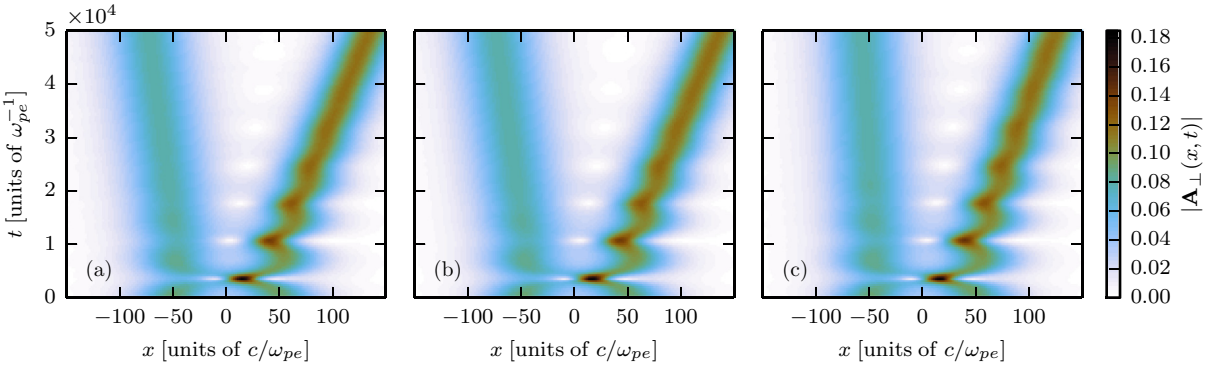

FIG. 5. (Color online) Comparison of simulations of two-soliton interaction with frequency $\omega_1 = \omega_2 = 0.999$, amplitude $R_0^{(1)} = R_0^{(2)} \simeq 0.0896$ (corresponding to $\epsilon \simeq 0.0447$, $k_1^{(1)} = k_1^{(2)} = 1$), initial distance $d_0 = 100$, and phase difference $\Psi_0 = 0.1\pi$, using (a) the fluid model Eq. (1), (b) pNLS Eq. (46), and (c) NLS Eq. (24).

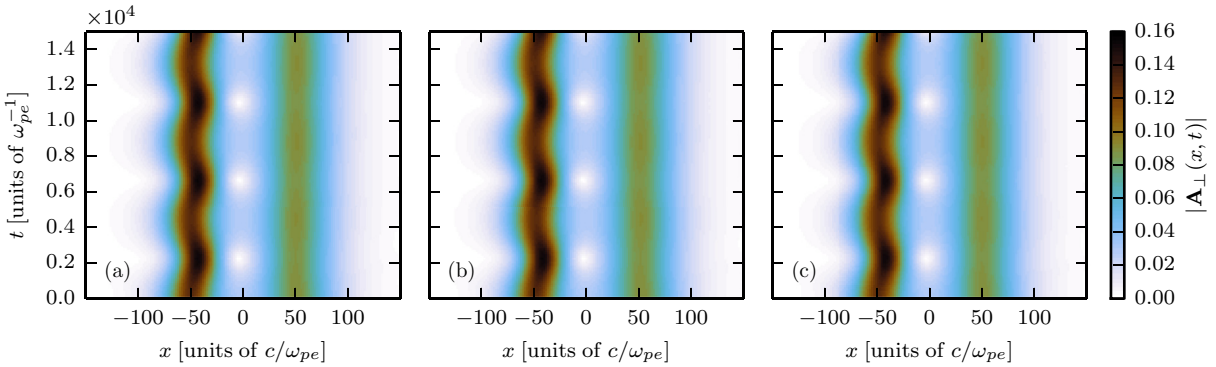

FIG. 6. (Color online) Comparison of simulations of two-soliton interaction with $\omega_1 = 0.999$, $R_0^{(1)} \simeq 0.0896$ and $\omega_2 = 0.998$, $R_0^{(2)} \simeq 0.127$ (corresponding to $\epsilon \simeq 0.0447$, $k_1^{(1)} = 1$, $k_1^{(2)} \simeq 1.4139$) and initial distance $d_0 = 100$ using (a) the fluid model Eq. (1), (b) pNLS Eq. (46), and (c) NLS Eq. (24).

opposite directions with velocities $v_L = -0.002$ and $v_R = 0.0021$ for the left and right moving soliton, respectively. The pNLS equation simulations agree with the fluid model predictions quantitatively, faithfully capturing the velocities of the outgoing solitons to be $v_L = -0.0024$ and $v_R = 0.0025$. On the other hand, NLS equation simulations exhibit oscillations in soliton position before the latter drift apart, a feature not present in the fluid simulations. Furthermore, the velocities of the outgoing solitons in the NLS equation simulations are $v_L = -0.0005$ and $v_R = 0.0007$, rather small compared to the fluid simulations.

Quasiparticle predictions for the distance of minimum approach $d_{\min}$ and corresponding time $t_{\min}$ are compared with the results of the numerical simulations in Table I, showing excellent agreement.

We also present the interaction of two solitons with $\omega_1 = \omega_2 = 0.99$ ($R_{0,1} = R_{0,2} \simeq 0.2879$, $\epsilon \simeq 0.1411$, $k_1^{(1)} = k_1^{(2)} = 1$), initial distance $d_0 = 60$, and very small phase difference $\Psi_0 = 10^{-6}$ in Fig. 10. In this case, $\Psi_0 < \Psi_c$, and indeed the two solitons do collide. However, after a subsequent recollision, they diverge and move away from each other. The pNLS equation simulations capture this feature, even though the velocities of the escaping solitons are much larger than in the fluid simulations. However, in the NLS equation simulations we see that the solitons keep recolliding for many iterations. Quasiparticle theory predicts that even for small initial phase difference the solitons will eventually drift apart; however, from Eq. (73) we find that the time scale required for this to happen for such a small initial phase difference is of the order of 10^9, well beyond the maximum integration time $t = 2 \times 10^5$ for which we could simulate the system.

The cold-fluid model conserves the normalized energy, $E = E_l + E_p + E_e$, where

$$E_l = \frac{1}{2}\int \left[\left(\frac{\partial A_y}{\partial t}\right)^2 + \left(\frac{\partial A_y}{\partial x}\right)^2 \right] dx, \tag{82}$$

$$E_p = \frac{1}{2}\int \left(\frac{\partial \phi}{\partial x}\right)^2 dx, \tag{83}$$

$$E_e = \int (\gamma - 1)\, n\, dx, \tag{84}$$

are electromagnetic, electrostatic, and kinetic energy contributions, respectively. In soliton collisions with a finite phase difference, energy can be transferred between the two solitons. We show this in Fig. 11, where we plot as a function of time the total energy E_{tot} in the computational domain and the energy E_L (E_R) in the left (right) half of the domain, for the cold-fluid model simulation of Fig. 10(a). We find that after the solitons separate, energy has been transferred to the soliton in the right half of the domain, while its amplitude has increased.

The results of Fig. 10 indicate that for larger amplitudes, cold-fluid-model-bound states do not persist under

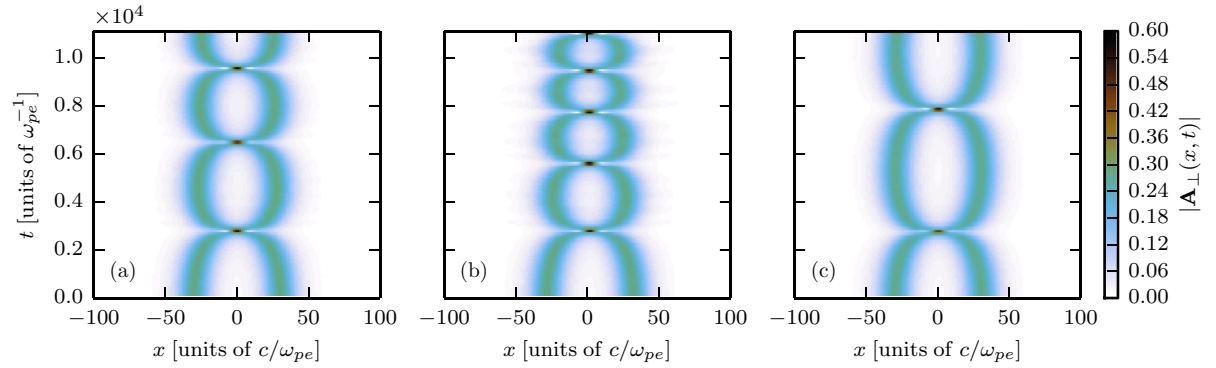

FIG. 7. (Color online) Comparison of simulations of soliton interaction with frequencies $\omega_1 = \omega_2 = 0.99$, amplitude $R_0^{(1)} = R_0^{(2)} \simeq 0.2879$ ($\epsilon \simeq 0.1411$, $k_1^{(1)} = k_1^{(2)} = 1$), and initial distance $d_0 = 60$, using (a) the fluid model Eq. (1), (b) pNLS Eq. (46), and (c) NLS Eq. (24).

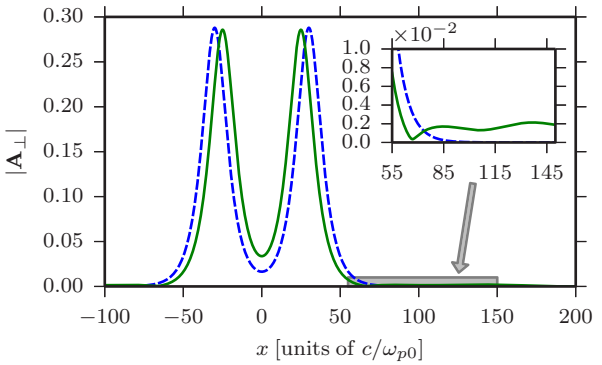

FIG. 8. (Color online) Two snapshots from cold-fluid model simulations of soliton interaction with frequencies $\omega_1 = \omega_2 = 0.99$, amplitude $R_0^{(1)} = R_0^{(2)} \simeq 0.2879$ ($\epsilon \simeq 0.1411$, $k_1^{(1)} = k_1^{(2)} = 1$), and initial distance $d_0 = 60$ [see also Fig. 7(a)]. Dashed (blue) line corresponds to $t = 0$; solid (green) line corresponds to $t \simeq 10745$, i.e., at maximum separation after the third collision. The inset corresponds to the area in the gray box.

perturbations involving phase difference of the two solitons, leading to qualitative difference from the NLS equation model dynamics. Figure 12 illustrates that the number of recollisions between solitons decreases as Ψ_0 increases. Such dynamics has been associated with chaotic scattering of solitons in the context of a perturbed NLS equation [43]. However, determining parameters for which chaotic scattering occurs in our problem is beyond the scope of this work. Figure 12 suggests that truncation error in simulations can lead to the breaking of a bound state, even when there is no initial phase difference, as we have observed in Ref. [24]. Therefore, we have taken care that simulations presented here are well resolved by checking that varying the spatial resolution does not affect the results.

3. *Solitary waves of unequal amplitude and no phase difference*

The case of solitons of frequencies $\omega_1 = 0.99$, $\omega_2 = 0.98$, amplitudes $R_0^{(1)} \simeq 0.2879$, $R_0^{(2)} \simeq 0.4144$ (corresponding to $\epsilon \simeq 0.1411$, $k_1^{(1)} = 1$, $k_1^{(2)} \simeq 1.4107$), initial distance $d_0 = 30$, and relative phase $\Psi_0 = 0$, is shown in Fig. 13. In this case, the solitons after some oscillations quickly diverge from each other. Simulations using the pNLS equation faithfully capture this behavior. On the contrary, NLS equation simulations show the formation of a bound state of oscillating solitons. We can therefore conclude that once again we have qualitative differences between cold-fluid model and NLS equation soliton interactions, with bound states appearing unstable within the former model.

TABLE I. Comparison of analytical prediction based on quasiparticle theory and results of numerical simulations of the different models studied here, for the distance of minimum approach $d_{\min}$ (in units of $c/\omega_{\rm pe}$) and corresponding time $t_{\min}$ (in units of $\omega_{\rm pe}^{-1}$), for two solitons of frequency $\omega_1 = \omega_2 = 0.99$, amplitude $R_0^{(1)} = R_0^{(2)} \simeq 0.2879$ ($\epsilon \simeq 0.1411$, $k_1^{(1)} = k_1^{(2)} = 1$), initial distance $d_0 = 60$, and initial phase difference $\Psi_0 = 0.1\pi$ (see Fig. 9).

	$d_{\min}$	$t_{\min}$
Quasiparticle (analytical)	40.5	2751.4
Fluid simulation	39.8	2703.0
pNLS equation simulation	39.7	2682.2
NLS equation simulation	40.0	2688.4

C. Cubic-quintic NLS equation approximation

Finally, we show that the qualitatively new features present in the larger amplitude simulations, may be captured by keeping only the quintic nonlinearity in Eq. (46), i.e., by the cubic-quintic NLS equation:

$$i\frac{\partial a}{\partial T} + \frac{1}{2}\frac{\partial^2 a}{\partial X^2} + |a|^2 a - 3\epsilon^2 |a|^4 a = 0. \qquad (85)$$

We present three different examples of soliton interaction dynamics under Eq. (85) in Fig. 14. In all cases, there is agreement at a qualitative level with cold-fluid model simulations of Eq. (85) of Sec. V B. This suggests that the "defocusing" quintic term induces the qualitative changes in soliton interactions. However, obtaining better quantitative agreement requires keeping all terms in Eq. (46), as in Sec. V B.

VI. DISCUSSION AND CONCLUSIONS

We studied weakly relativistic bright solitons and their interactions using a perturbative, multiple scale analysis and

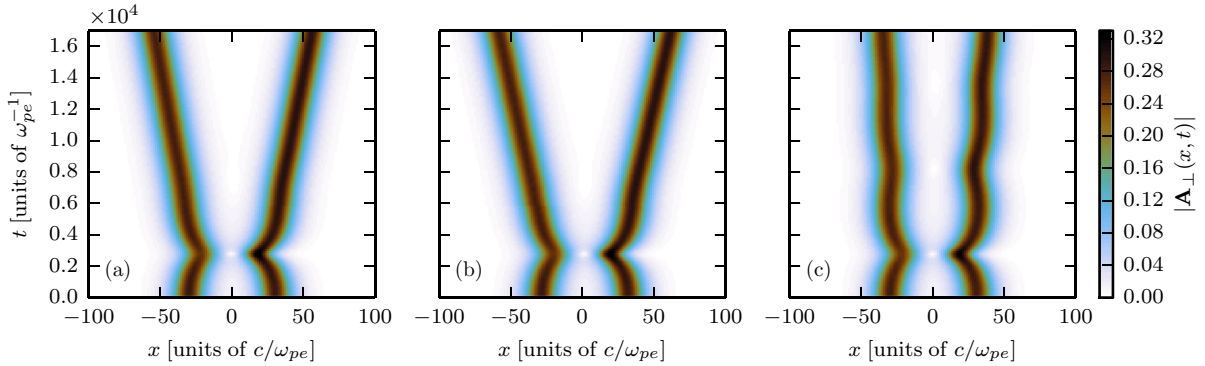

FIG. 9. (Color online) Comparison of simulations of two-soliton interaction with frequency $\omega_1 = \omega_2 = 0.99$ (amplitude $R_0^{(1)} = R_0^{(2)} \simeq 0.2879$, $\epsilon \simeq 0.1411$, $k_1^{(1)} = k_1^{(2)} = 1$), initial distance $d_0 = 60$, and phase difference $\Psi_0 = 0.1\pi$, using (a) the fluid model Eq. (1), (b) pNLS Eq. (46), and (c) NLS Eq. (24).

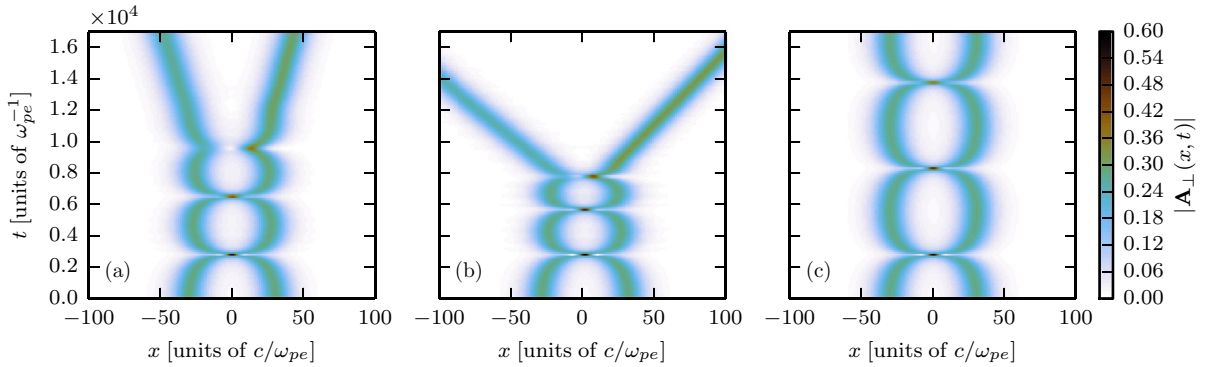

FIG. 10. (Color online) Comparison of simulations of two-soliton interaction with frequency $\omega_1 = \omega_2 = 0.99$, amplitude $R_0^{(1)} = R_0^{(2)} \simeq 0.2879$ ($\epsilon \simeq 0.1411$, $k_1^{(1)} = k_1^{(2)} = 1$), initial distance $d_0 = 60$, and phase difference $\Psi_0 = 10^{-6}$, using (a) the fluid model Eq. (1), (b) pNLS Eq. (46), and (c) NLS Eq. (24).

direct numerical simulations. We derived an equation for the evolution of the field envelope valid for small amplitudes, keeping terms up to order five in the small parameter.

Localization of the soliton solutions appears naturally in our scheme through the requirement $\omega \lesssim \omega_{\rm pe}$, obtained through the linear dispersion relation. The lowest-order nonlinear effect is due to the relativistic nonlinearity, leading to a classical cubic NLS equation. The cubic nonlinearity balances pulse dispersion, leading to the formation of solitons. However, higher-order terms, most importantly the quintic term resulting from the expansion of the relativistic nonlinearity, become essential at larger amplitudes. In particular, the response of the plasma to the ponderomotive force and the formation of a density cavitation, which confines the soliton, is only captured by keeping fifth-order terms in the small parameter, leading to the pNLS Eq. (46). At even higher amplitudes, soliton width becomes comparable to the wavelength of the carrier electromagnetic wave and the perturbative description breaks down.

We have demonstrated the utility of the NLS and pNLS equations derived here by applying them to the problem of standing solitary wave interaction. We have found that the lowest-order NLS equation approximation works very well for lower amplitudes but gives qualitatively different results at higher amplitudes. For well-separated solitons, the quasiparticle approach provides analytical estimates for the first collision time and minimum distance of approach of two solitons. We have found that these estimates are in very good agreement with fluid simulations, even for larger amplitudes. The reason for this is that the overlapping part of well-separated relativistic solitons can be well approximated by the tails of NLS equation solitons. The effect of higher-order terms that leads, e.g., to inelastic collisions, only becomes significant after the solitons have approached each other.

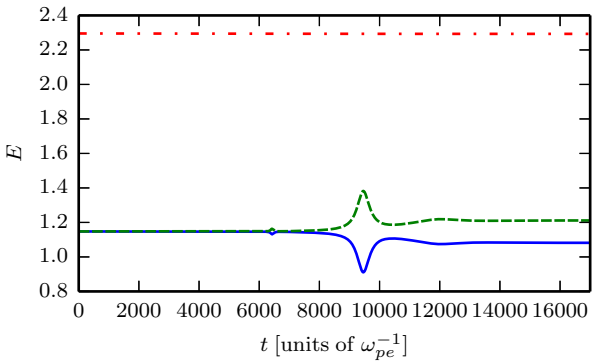

FIG. 11. (Color online) Total energy $E_{\rm tot}$ in the computational domain (red, dot-dashed line) and energy E_L (blue, solid line) and E_R (green, dashed line) in the left and right half of the domain, respectively, corresponding to cold-fluid model simulation described in the legend of Fig. 10(a).

Once the solitons are sufficiently close to each other, the higher-order terms become important and lead to qualitatively different results than in the NLS equation. For example, since the NLS equation is a completely integrable equation, its soliton collisions are elastic. However, in our fluid simulations we have clear signatures of inelastic soliton collisions accompanied by emission of radiation. These features are captured qualitatively by keeping the higher-order terms in the pNLS equation. We can attribute the emission of radiation in collisions to the role of the "defocusing" fifth-order nonlinearity. In cases in which the total amplitude of the field remains in the perturbative regime, good quantitative agreement is obtained between the cold-fluid and pNLS equation simulations. Our study suggests that the collision time for well-separated solitons can become larger than the typical response time of the ions $(m_i/m_e)^{1/2}\ 2\pi\ /\omega_{\rm pe}$, where m_i is the ion mass [8], and ion dynamics would have to be taken into account in future studies.

As we have seen in Fig. 11, one feature of soliton collisions is the transfer of energy from one soliton to the other during the interaction. Moreover, it can be seen in Fig. 10 that the wave on the right-hand side has a larger amplitude after the collision. This is interesting in connection to wave-breaking of solitons, which occurs above a certain amplitude threshold and has been proposed in the past as a means to accelerate particles [5,19]. Our simulations indicate that soliton interaction is a good candidate to trigger wave-breaking, through which electromagnetic energy of the wave could be transferred to the particles.

The introduction of NLS equation as the lowest-order approximation to the problem of relativistic solitary interaction allowed the application of quasiparticle theory of NLS

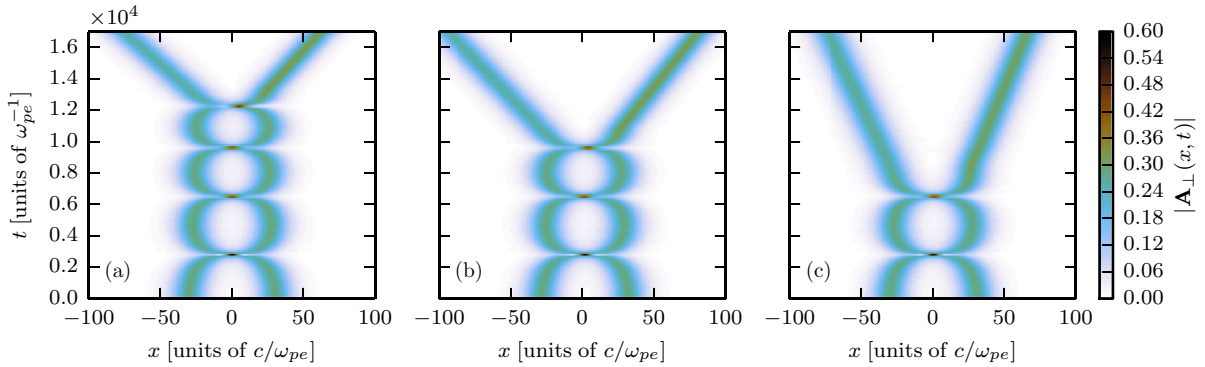

FIG. 12. (Color online) Cold fluid model simulations of two-soliton interaction with frequency $\omega_1 = \omega_2 = 0.99$, amplitude $R_0^{(1)} = R_0^{(2)} \simeq 0.2879$ ($\epsilon \simeq 0.1411$, $k_1^{(1)} = k_1^{(2)} = 1$), initial distance $d_0 = 60$, and phase difference using (a) $\Psi_0 = 10^{-9}$, (b) $\Psi_0 = 10^{-7}$, (c) $\Psi_0 = 10^{-5}$.

equation solitons in order to obtain analytical estimates for collision time and minimum distance of approach. The development of the pNLS equation framework, on the other hand, suggests the possibility to use further mathematical tools such as the inverse scattering transform (IST) [25]. For instance, in the context of Alfvén waves, IST applied to the derivative-NLS equation was used to explain the collapse of the bright Alfvén soliton and the formation of robust magnetic holes [44,45]. The model derived here suggests that the IST of the NLS equation could be used in a similar manner to analyze simulations and get insight on the interaction and disappearance of solitons in laser-plasma interaction.

In summary, a perturbed NLS equation describing electromagnetic envelope evolution for weakly relativistic pulses in plasmas has been derived. Auxiliary equations describe the plasma density, momentum, and electrostatic potential in terms of the electromagnetic field. The pNLS model agrees very well with fluid model simulations of soliton interactions. Our simulations suggest that in the small but finite amplitude regime the defocusing quintic nonlinearity becomes important and soliton collisions are inelastic.

ACKNOWLEDGMENTS

E.S. thanks S. Skupin and F. Maucher for helpful suggestions. Work by G.S. was supported by the Ministerio de Economía y Competitividad of Spain (Grant No. ENE2011-28489). We thank the anonymous referees for many useful suggestions.

APPENDIX A: RELATION OF FLUID MODEL AND ENVELOPE INITIAL CONDITIONS

Here, we specify how initial conditions of the cold-fluid model are related to initial conditions of the pNLS equation. Letting $a = a_r + i\, a_i$, we note that Eqs. (2a), (2b), and (11), with the help of $a = -i\, b$, give

$$A_y(x,t) = 2\epsilon\, [a_r(X,T)\, \cos\, t + a_i(X,T) \sin\, t]\,, \quad \text{(A1a)}$$

$$A_z(x,t) = 2\epsilon\, [-a_i(X,T)\, \cos\, t + a_r(X,T) \sin\, t]\,, \quad \text{(A1b)}$$

or

$$a_r(X,T) = \frac{1}{2\epsilon}(A_y\, \cos\, t + A_z \sin\, t), \quad \text{(A2a)}$$

$$a_i(X,T) = \frac{1}{2\epsilon}(-A_z \cos\, t + A_y\, \sin\, t). \quad \text{(A2b)}$$

Setting $T = t = 0$, we get

$$a_r(X,0) = \frac{1}{2\epsilon} A_y(x,0), \quad \text{(A3a)}$$

$$a_i(X,0) = -\frac{1}{2\epsilon} A_z(x,0). \quad \text{(A3b)}$$

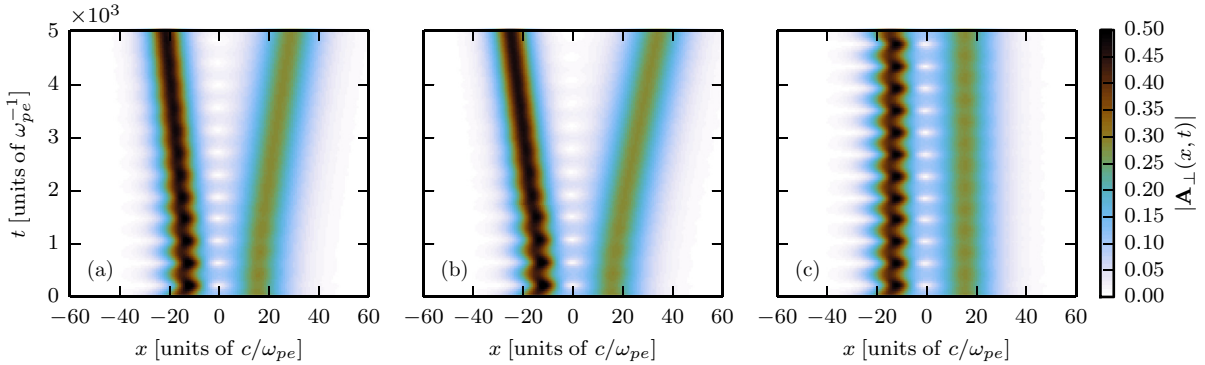

FIG. 13. (Color online) Comparison of simulations of two-soliton interaction with frequencies $\omega_1 = 0.99$, $\omega_2 = 0.98$, amplitudes $R_0^{(1)} \simeq 0.2879$, $R_0^{(2)} \simeq 0.4144$ (corresponding to $\epsilon \simeq 0.1411$, $k_1^{(1)} = 1$, $k_1^{(2)} \simeq 1.4107$), initial distance $d_0 = 30$, and relative phase $\Psi_0 = 0$ using (a) the fluid model Eq. (1), (b) pNLS Eq. (46), and (c) NLS Eq. (24).

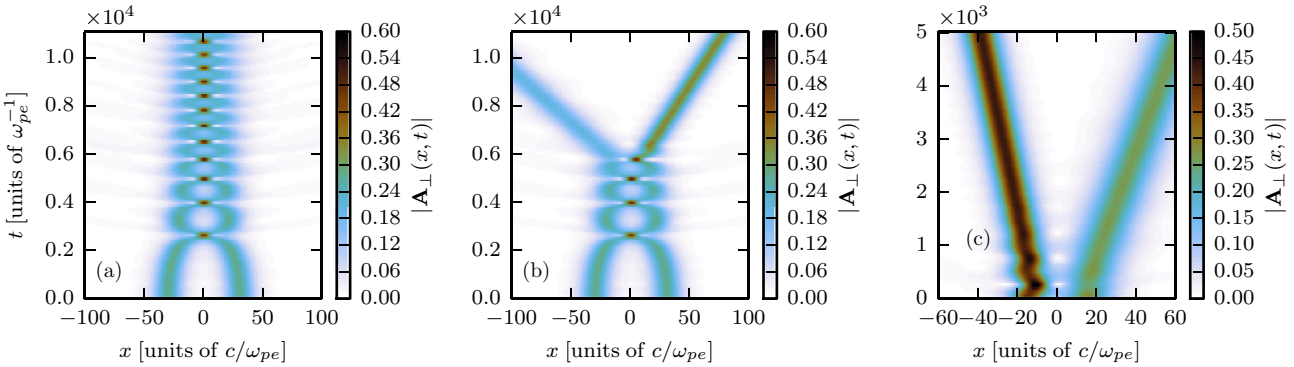

FIG. 14. (Color online) Solitary wave interaction using the cubic-quintic NLS equation approximation Eq. (85) for two solitons with (a) frequencies $\omega_1 = \omega_2 = 0.99$, amplitudes $R_0^{(1)} = R_0^{(2)} \simeq 0.288$, and initial distance $d_0 = 60$, as described in the legend of Fig. 7, (b) frequencies $\omega_1 = \omega_2 = 0.99$, amplitudes $R_0^{(1)} = R_0^{(2)} \simeq 0.288$, initial distance $d_0 = 60$, and phase difference $\Psi_0 = 10^{-6}$, as described in the legend of Fig. 9, and (c) frequencies $\omega_1 = 0.99$, $\omega_2 = 0.98$ ($R_0^{(1)} \simeq 0.288$ and $R_0^{(2)} \simeq 0.414$), and initial distance $d_0 = 30$, as described in the legend of Fig. 13.

Using Eq. (10) in Eq. (A2), we arrive at

$$a_r = \frac{1}{2\epsilon}\Bigg[A_y \cos\omega t \cos\left(\frac{|k_1|^2}{2}T\right) - A_y \sin\omega t \sin\left(\frac{|k_1|^2}{2}T\right) + A_z \sin\omega t \cos\left(\frac{|k_1|^2 T}{2}\right) + A_z \cos\omega t \sin\left(\frac{|k_1|^2}{2}T\right)\Bigg], \tag{A4a}$$

$$a_i = \frac{1}{2\epsilon}\Bigg[-A_z \cos\omega t \cos\left(\frac{|k_1|^2}{2}T\right) + A_z \sin\omega t \sin\left(\frac{|k_1|^2}{2}T\right) + A_y \sin\omega t \cos\left(\frac{|k_1|^2 T}{2}\right) + A_y \cos\omega t \sin\left(\frac{|k_1|^2}{2}T\right)\Bigg]. \tag{A4b}$$

Taking the derivative of Eq. (A4) with respect to T and setting $t = T = 0$, we get

$$\left.\frac{\partial a_r}{\partial T}\right|_{T=0} = \frac{A_z(x,0)}{4\epsilon}|k_1|^2, \tag{A5a}$$

$$\left.\frac{\partial a_i}{\partial T}\right|_{T=0} = \frac{A_y(x,0)}{4\epsilon}|k_1|^2. \tag{A5b}$$

APPENDIX B: NUMERICAL SOLUTION OF FLUID EQUATIONS

For the numerical solution of the fluid system we chose to use spectral (Fourier) discretization of the field and plasma quantities, while time stepping is handled by an adaptive fourth-order Runge-Kutta scheme. This necessitates the introduction of the components of the electric field, in order to arrive at partial differential equations involving only first-time derivatives. Specifically, we write the longitudinal component of Ampere's law as

$$\frac{\partial E_x}{\partial t} = \frac{N}{\gamma}P_x, \tag{B1}$$

while the wave equation is split into

$$\frac{\partial \mathbf{E}_\perp}{\partial t} = -\frac{\partial^2 \mathbf{A}_\perp}{\partial x^2} + \frac{N}{\gamma}\mathbf{A}_\perp, \tag{B2}$$

and

$$\frac{\partial \mathbf{A}_\perp}{\partial t} = -\mathbf{E}_\perp. \tag{B3}$$

The momentum equation yields simply

$$\frac{\partial P_x}{\partial t} = -E_x - \frac{\partial \gamma}{\partial x}. \tag{B4}$$

Instead of solving Poisson Eq. (1d), we introduce the continuity equation in order to determine the rate of change of density,

$$\frac{\partial N}{\partial t} = -\frac{\partial}{\partial x}\left(\frac{N P_x}{\gamma}\right). \tag{B5}$$

Finally, using Eq. (1e) we derive an equation for the rate of change of γ,

$$\frac{\partial \gamma}{\partial t} = -\frac{1}{\gamma}\left[P_x\left(E_x + \frac{\partial \gamma}{\partial x}\right) + A_y E_y + A_z E_z\right]. \tag{B6}$$

[1] A. Akhiezer and R. Polovin, Sov. Phys. JETP **3**, 696 (1956).
[2] J. H. Marburger and R. F. Tooper, Phys. Rev. Lett. **35**, 1001 (1975).
[3] V. A. Kozlov, A. G. Litvak, and E. V. Suvorov, Sov. Phys. JETP **49**, 75 (1979).
[4] P. K. Kaw, A. Sen, and T. Katsouleas, Phys. Rev. Lett. **68**, 3172 (1992).

[5] T. Esirkepov, F. Kamenets, S. Bulanov, and N. Naumova, JETP Lett. **68**, 36 (1998).

[6] S. V. Bulanov, I. N. Inovenkov, V. I. Kirsanov, N. M. Naumova, and A. S. Sakharov, Phys. Fluids B **4**, 1935 (1992).

[7] S. V. Bulanov, T. Z. Esirkepov, N. M. Naumova, F. Pegoraro, and V. A. Vshivkov, Phys. Rev. Lett. **82**, 3440 (1999).

[8] N. M. Naumova, S. V. Bulanov, T. Z. Esirkepov, D. Farina, K. Nishihara, F. Pegoraro, H. Ruhl, and A. S. Sakharov, Phys. Rev. Lett. **87**, 185004 (2001).

[9] T. Esirkepov, K. Nishihara, S. V. Bulanov, and F. Pegoraro, Phys. Rev. Lett. **89**, 275002 (2002).

[10] S. S. Bulanov, T. Z. Esirkepov, F. F. Kamenets, and F. Pegoraro, Phys. Rev. E **73**, 036408 (2006).

[11] D. Wu, C. Y. Zheng, X. Q. Yan, M. Y. Yu, and X. T. He, Phys. Plasmas **20**, 033101 (2013).

[12] M. Borghesi, S. Bulanov, D. H. Campbell, R. J. Clarke, T. Z. Esirkepov, M. Galimberti, L. A. Gizzi, A. J. MacKinnon, N. M. Naumova, F. Pegoraro, H. Ruhl, A. Schiavi, and O. Willi, Phys. Rev. Lett. **88**, 135002 (2002).

[13] L. Romagnani, A. Bigongiari, S. Kar, S. V. Bulanov, C. A. Cecchetti, T. Z. Esirkepov, M. Galimberti, R. Jung, T. V. Liseykina, A. Macchi, J. Osterholz, F. Pegoraro, O. Willi, and M. Borghesi, Phys. Rev. Lett. **105**, 175002 (2010).

[14] G. Sarri, D. K. Singh, J. R. Davies, F. Fiuza, K. L. Lancaster, E. L. Clark, S. Hassan, J. Jiang, N. Kageiwa, N. Lopes, A. Rehman, C. Russo, R. H. H. Scott, T. Tanimoto, Z. Najmudin, K. A. Tanaka, M. Tatarakis, M. Borghesi, and P. A. Norreys, Phys. Rev. Lett. **105**, 175007 (2010).

[15] G. Sarri, S. Kar, L. Romagnani, S. V. Bulanov, C. A. Cecchetti, M. Galimberti, L. A. Gizzi, R. Heathcote, R. Jung, I. Kourakis, J. Osterholz, A. Schiavi, O. Willi, and M. Borghesi, Phys. Plasmas **18**, 080704 (2011).

[16] L. M. Chen, H. Kotaki, K. Nakajima, J. Koga, S. V. Bulanov, T. Tajima, Y. Q. Gu, H. S. Peng, X. X. Wang, T. S. Wen, H. J. Liu, C. Y. Jiao, C. G. Zhang, X. J. Huang, Y. Guo, K. N. Zhou, J. F. Hua, W. M. An, C. X. Tang, and Y. Z. Lin, Phys. Plasmas **14**, 040703 (2007).

[17] A. S. Pirozhkov, J. Ma, M. Kando, T. Z. Esirkepov, Y. Fukuda, L.-M. Chen, I. Daito, K. Ogura, T. Homma, Y. Hayashi, H. Kotaki, A. Sagisaka, M. Mori, J. K. Koga, T. Kawachi, H. Daido, S. V. Bulanov, T. Kimura, Y. Kato, and T. Tajima, Phys. Plasmas **14**, 123106 (2007).

[18] F. Sylla, A. Flacco, S. Kahaly, M. Veltcheva, A. Lifschitz, G. Sanchez-Arriaga, E. Lefebvre, and V. Malka, Phys. Rev. Lett. **108**, 115003 (2012).

[19] D. Farina and S. V. Bulanov, Phys. Rev. Lett. **86**, 5289 (2001).

[20] D. Farina and S. V. Bulanov, Plasma Phys. Contr. Fusion **47**, A73 (2005).

[21] G. Sanchez-Arriaga, E. Siminos, and E. Lefebvre, Phys. Plasmas **18**, 082304 (2011).

[22] G. Sánchez-Arriaga, E. Siminos, and E. Lefebvre, Plasma Phys. Contr. Fusion **53**, 045011 (2011).

[23] S. V. Bulanov, F. Califano, T. Z. Esirkepov, K. Mima, N. M. Naumova, K. Nishihara, F. Pegoraro, Y. Sentoku, and V. A. Vshivkov, Physica D **152**, 682 (2001).

[24] V. Saxena, I. Kourakis, G. Sanchez-Arriaga, and E. Siminos, Phys. Lett. A **377**, 473 (2013).

[25] A. Hasegawa and Y. Kodama, *Solitons in Optical Communications* (Clarendon Press, Oxford, 1995).

[26] T. Taniuti and N. Yajima, J. Math. Phys. **10**, 1369 (1969).

[27] T. Dauxois and M. Peyrard, *Physics of solitons* (Cambridge University Press, Cambridge, UK, 2006).

[28] R. Hoyle, *Pattern Formation: An Introduction to Methods* (Cambridge University Press, Cambridge, 2006).

[29] A. P. Fordy, in *Soliton Theory: A Survey of Results*, edited by A. P. Fordy (Manchester University Press, Manchester, UK, 1990), Chap. 15.

[30] A. C. Scott, F. Chu, and D. McLaughlin, P. IEEE **61**, 1443 (1973).

[31] K. B. Dysthe and K. Trulsen, Phys. Scr. **T82**, 48 (1999).

[32] G. P. Veldes, J. Borhanian, M. McKerr, V. Saxena, D. J. Frantzeskakis, and I. Kourakis, J. Opt. **15**, 064003 (2013).

[33] A. C. Newell and J. V. Moloney, *Nonlinear Optics* (Addison-Wesley, Redwood City, CA, 1992).

[34] I. Kourakis and P. K. Shukla, Nonlin. Processes Geophys. **12**, 407 (2005).

[35] R. E. Kates and D. J. Kaup, J. Plasma Phys. **42**, 507 (1989).

[36] H. H. Kuehl, C. Y. Zhang, and T. Katsouleas, Phys. Rev. E **47**, 1249 (1993).

[37] H. H. Kuehl and C. Y. Zhang, Phys. Rev. E **48**, 1316 (1993).

[38] P. Gibbon, *Short Pulse Laser Interactions with Matter* (Imperial College Press, London, 2005).

[39] C. Sulem and P.-L. Sulem, *The Nonlinear Schrödinger Equation. Self-Focusing and Wave Collapse*, Applied Mathematical Sciences, Vol. 139 (Springer, New York, 1999).

[40] V. I. Karpman and V. V. Solov'ev, Physica D **3**, 487 (1981).

[41] J. P. Gordon, Opt. Lett. **8**, 596 (1983).

[42] G. R. Dennis, J. J. Hope, and M. T. Johnsson, Comp. Phys. Commun. **184**, 201 (2013).

[43] S. V. Dmitriev, D. A. Semagin, A. A. Sukhorukov, and T. Shigenari, Phys. Rev. E **66**, 046609 (2002).

[44] G. Sánchez-Arriaga, D. Laveder, T. Passot, and P. L. Sulem, Phys. Rev. E **82**, 016406 (2010).

[45] G. Sánchez-Arriaga, Phys. Plasmas **17**, 082313 (2010).